Optics & Laser Technology 143 (2021) 107367

Contents lists available at ScienceDirect

Optics and Laser Technology

journal homepage: www.elsevier.com/locate/optlastec

Generation of one-dimensional vortex-arrays with tunable singularity and high peak power in a passively Q-switched microchip laser

Xiaocan Wang [a], Shengchuang Bai [a], Yue Pan [a], Bohan Lin [b], Jun Dong [a,*]

[a] Laboratory of Laser and Applied Photonics (LLAP), Department of Electronic Engineering, School of Electronic Science and Engineering, Xiamen University, Xiamen 361005, PR China

[b] School of Information Science and Technology, Xiamen University Malaysia, Sepang, Selangor Darul Ehsan 43900, Malaysia

ARTICLE INFO

Keywords:
Vortex arrays
passively Q-switched
Singularity
Microchip laser
Decentered annular beam

ABSTRACT

One-dimensional (1D) vortex-arrays with multiple-singularity aligning along a line are flexible for microparticle manipulation, high capacity storage, material processing. Moreover, a high peak power one-dimensional vortex-array with large singularity enables assemble processing. The development of a miniature laser to directly generate one-dimensional vortex-array with tunable singularity is of great value for practical applications. However, solid-state lasers for this purpose was limited by the low power, low efficiency and less singularity achieved. Here, we demonstrate a simple and robust method for directly generating one-dimensional vortex-array with singularity tunable upon to 4 in a tilted Nd:YAG/Cr^{4+}:YAG composite crystal passively Q-switched (PQS) microchip laser, irradiated by a decentered annular beam (DAB). The singularity of one-dimensional vortex-array can be tuned from 1 to 4 by controlling the offset of collimating lens, Δx. The average output power of one-dimensional vortex-array with 4 singularities is 0.76 W at P_{in} = 5.66 W, the optical conversion efficiency is 13.4%. One-dimensional vortex-array with 4 singularities processes pulse width of 3.5 ns, peak power of 5.56 kW. The achieved results suggest the potential that DAB can be used a practical pump beam in PQS microchip laser for generating nanosecond, high peak power one-dimensional vortex-arrays with tunable singularity.

1. Introduction

Optical vortices with optical angular momentum (OAM) have been demonstrated to have potential applications in quantum entanglement [1,2], optical tweezers [3–7], and optical communication [8–12]. The Laguerre-Gaussian ($LG_{0,n}$) modes, the most common vortex beams, have been investigated extensively in recent years. However, $LG_{0,n}$ mode vortices have only one singularity and many applications are limited by the simple spatial structure of such vortices. The multi-vortex modes, especially one-dimensional vortex-arrays with multiple singularity aligning along a line, have attracted great attention. The multi-vortex modes with unique characteristics of structured light fields and multiple singularities offer more flexibility for optical communication and manipulating particles. The dual-vortex lasers have been demonstrated using the methods such as mode superposition [13], a spatial light modulator [14] and the second-harmonic generation utilizing sub-picosecond pulses [15]. However, formation of dual-vortex laser with external optical elements makes the lasers more complicated and less efficient, and practical applications of such dual-vortex lasers are restricted with less portability, less flexibility, low damage threshold. Other types of multi-vortex beams such as fractional OAM beams, multiple closed-packed optical vortex beams were also reported [16–21]. Spatial light modulator [16,20], spiral phase plate, two-level pure-phase diffractive optical element [20] and mode converter [19] were used to generate vortex-arrays with multiple singularity. Meanwhile, some theoretical results of multi-vortex beams have been also reported [21–25]. A singularity hybrid evolution nature sphere was introduced recently [21] for five singularities via a $\pi/2$ astigmatic mode converter. However, the continuous-wave operation of these vortex-array lasers with low output power and complex laser system may greatly restrict practical applications. Therefore, pulsed vortex-array lasers with high peak power are extremely needed for practical applications such as manipulation of microparticles, assemble material processing.

The annular beam pumping provides a new way to generate vortex beams in microchip lasers owing to the good mode matching [26–31].

* Corresponding author.
E-mail address: jdong@xmu.edu.cn (J. Dong).

https://doi.org/10.1016/j.optlastec.2021.107367
Received 17 February 2021; Received in revised form 12 April 2021; Accepted 22 June 2021
Available online 30 June 2021
0030-3992/© 2021 Elsevier Ltd. All rights reserved.

However, the mode conversion efficiency from a laser diode with Gaussian distribution to an annular beam is low by using axicon [26], mode-conversion fiber [27], fiber capillary [28,29]. An annular beam formed with a hollow focus lens (HFL) has been demonstrated to be an efficient method [30]. Annular beams formed with HFL or beam shaping from a laser diode [31] have been successfully used to pump Nd:YAG and Yb:YAG microchip lasers for directly generating vector vortex beams and vortex arrays [30,32,33]. Nanosecond, high peak power vortex laser has been generated in a Cr,Nd:YAG self-Q-switched microchip laser pumped with an annular beam formed with a HFL [34]. Moreover, a decentered Gaussian beam pumped Nd:YAG/Cr^{4+}:YAG passively Q-switched (PQS) microchip laser has been demonstrated for generating LG, HG and IG modes [35]. The decentered beam pumping breaks the symmetry of the laser cavity and provides possibilities for multi-transverse modes oscillation. The tilted beam pumping has the same effect as the decentered beam pumping [36], and can further increase the inversion population distribution along one direction. Recently, we demonstrated a decentered annular beam (DAB) pumped Nd:YAG/Cr^{4+}:YAG PQS microchip laser for generating dual-vortex laser, and the separation and orientation of two vortices were controlled by adjusting the offset of collimating lens along *x*-axis and *y*-axis [37]. However, dual-vortex PQS microchip laser with two singularities still has a long way for applications on assemble processing of quantum information, large capacity storage and material processing. Therefore, pulsed vortex-array lasers with more singularities aligning along a line are extremely needed to be investigated to fulfill various applications.

Here, we demonstrated a simple and solid method for directly generating high peak power one-dimensional vortex-arrays with tunable singularity in a DAB pumped tilted Nd:YAG/Cr^{4+}:YAG PQS microchip laser. The singularity of one-dimensional vortex-array is tuned from 1 to 4 by controlling the offset of collimating lens, Δx, in collimating and focusing optical system. The average output power of one-dimensional vortex-array with four singularities was 0.76 W when the incident pump power (P_{in}) was 5.66 W. The optical-to-optical efficiency was 13.4%. The pulse width and peak power are 3.5 ns in fall width at half maximum (FWHM) and 5.56 kW, respectively.

2. Experiment

The experimental schematic of DAB pumped tilted Nd:YAG/Cr^{4+}:YAG PQS microchip laser for generating singularity tunable one-dimensional vortex-arrays is shown in Fig. 1. The pump source was an 808 nm fiber-coupled laser diode (LD) with a core diameter of 400 μm and a numerical aperture of 0.22. With a collimating lens (CF) and an HFL, the light from fiber was converted into an annular beam. The focal lengths of CL and HFL were 8 mm. The focus spot was about 170 μm in diameter. The distance between the focal spot and the rear surface of the composite crystal was 0.3 mm. DAB was formed by offsetting CL away from the *z*-axis along *x*-axis. The offset of CL along *x*-axis is labeled as Δx while the offset of CL along *y*-axis is 0. The laser material is a composite crystal fabricated with a 3-mm-thick 1 at.% Nd:YAG crystal and a 0.5-mm-thick Cr^{4+}:YAG crystal with an initial transmission of 90%. High-reflection coating at 1064 nm was deposited on Nd:YAG surface to work as the rear cavity mirror. Anti-reflection coating at 1064 nm was deposited on Cr^{4+}:YAG surface to eliminate intracavity loss. The output coupler (OC) is a plane-parallel mirror with reflection of 70% at 1064 nm and tilted 0.5° with respect to Nd:YAG/Cr^{4+}:YAG composite crystal for achieving stable chirality. The laser resonator was placed obliquely with respect to the *x*-axis, and the inclination angle β was 1°. The laser experiment was carried out at room temperature without active cooling system. The average output power was measured with a Thorlabs PM200 power meter. The laser pulse characteristics were detected with a 5 GHz InGaAs photo-diode and recorded with a 1 GHz bandwidth Tektronix digital phosphor oscilloscope (MDO3104). A Thorlabs BC106-VIS beam profiler was used to monitor the beam intensity profile. The phase structures of the one-dimensional vortex-arrays were checked with a home-made Mach-Zehnder interferometer.

3. Results

3.1. Transverse intensity profiles

A. Tilted PQS microchip laser

Firstly, the intensity profiles of tilted PQS microchip laser were measured when the CL and HFL were aligned along the beam propagation direction of fiber coupled LD ($\Delta x = 0$). The laser oscillated in a doughnut mode when the P_{in} reached 1.35 W. The evolution of the transverse intensity profiles with P_{in} is shown in column I for $\Delta x = 0$ in Fig. 2. The doughnut-shaped transverse intensity profile was kept when P_{in} gradually increased from 1.35 W to 3 W, as shown in column I in Fig. 2(a) and (b). Further increasing P_{in} exceeding 3 W, the transverse intensity profile tends to extend along *x*-axis and exhibits an elliptical distribution, one typical example is shown in column I in Fig. 2(c). The elliptical transverse intensity profile tends to further elongate with increase in P_{in}. A typical two-hole transverse intensity profile is shown in column I in Fig. 2(d). Therefore, pump power-dependent laser beams with doughnut and two-hole transverse intensity profiles were obtained in tilted PQS microchip laser.

B. DAB pumped tilted PQS microchip laser

Then, the DAB pumped tilted PQS microchip laser was investigated by increasing Δx of the CL. When Δx is increased to 40 μm, CL is at the position (40,0), the threshold pump power increases because the pump beam diameter of DAB is expanded and more pump power is needed for laser oscillation. The laser intensity profiles at different P_{in}s are shown in column II in Fig. 2. The laser intensity profile with a two-vortex was observed at $P_{in} = 2.48$ W. The PQS microchip laser still oscillated in two-vortex with further increase in P_{in}, as shown in column II in Fig. 2. However, the separation of the two vortices becomes smaller with increase in P_{in}, which is attributed to the enhanced pump power intensity at the central pump area due to the increase of the P_{in} at the same pump beam diameter. When Δx is further increased to 80 μm, the CL is at position of (80,0), the laser intensity profile with three-vortex is observed at P_{in} higher than 3 W. The three-vortex laser oscillated with

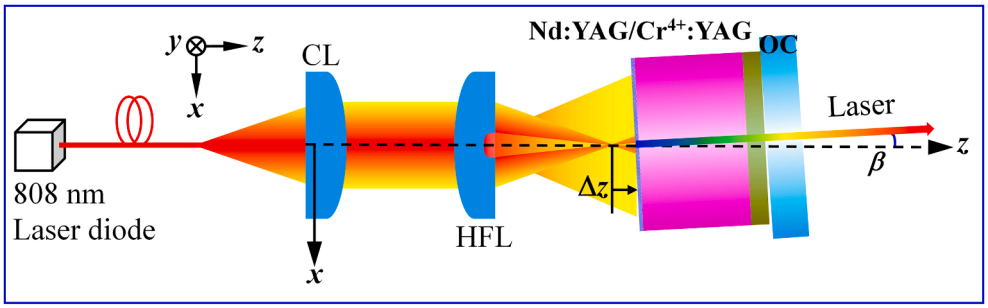

Fig. 1. Schematic of DAB pumped tilted PQS microchip laser. CL: collimating lens, HFL: hollow focus lens, OC: output coupler.

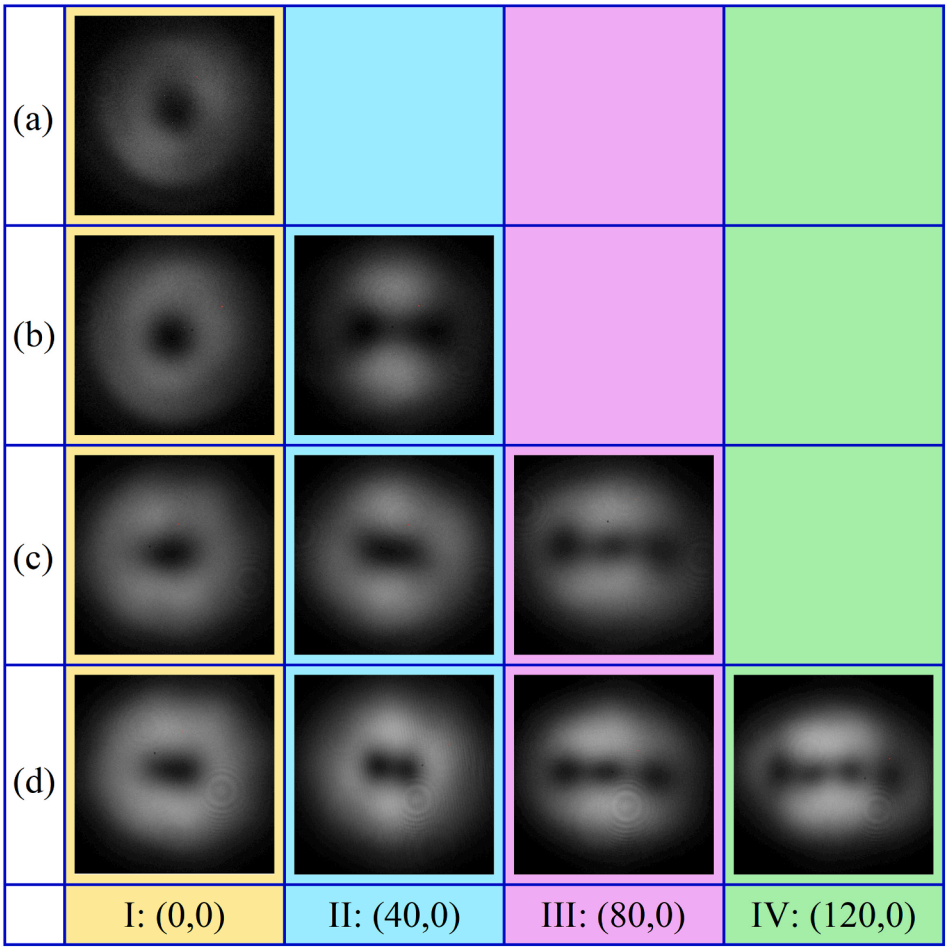

Fig. 2. Typical one-dimensional vortex-arrays with tunable singularity obtained experimentally in DAB pumped tilted PQS microchip laser at different P_{in}: (a) 1.37 W, (b) 2.48 W, (c) 3.81 W, (d) 5.21 W. (Δx,0) indicates the position of CL, I: $\Delta x = 0$, II: $\Delta x = 40$ μm, III: $\Delta x = 80$ μm, IV: $\Delta x = 120$ μm.

increase in P_{in}, as shown in column III in Fig. 2. Further increasing Δx to 120 μm, the CL is at the position of (120,0), four-vortex laser intensity profile is obtained when P_{in} reaches 5 W. One typical four-vortex laser intensity profile is shown in column IV in Fig. 2. Therefore, one-dimensional vortex-arrays were generated in the DAB pumped titled PQS microchip laser.

3.2. Phase structures

The phase structures of the obtained vortices and vortex-arrays at different positions (Δx,0) and P_{in}s were checked with a home-made Mach-Zehnder interferometer. The obtained laser beams were interfered with a plane-wave reference beam formed by selecting a small portion from the obtained laser beam with an aperture. For laser beams with single vortex distribution, the interference patterns exhibit one fringe splitting to two fringes at dislocation, as shown in column I in Fig. 3. For the laser beams with two vortices, the interference patterns clearly show that there are two opposite forklike fringes, as shown in column II in Fig. 3. The interference patterns of laser intensity profiles with three vortices, as shown in column III in Fig. 3, clearly show there are three forklike fringes aligned along one line, and the direction of forklike fringes is opposite between the adjacent vortices. The interference pattern of laser intensity profile with four vortices, as shown in column IV in Fig. 3, exhibits four forklike fringes along on line, and the direction of the adjacent forklike fringes is opposite. The interference patterns further confirm that the obtained vortex and vortex-arrays possess one singularity and tunable singularity from two to four depending on the applied pump power and offset distance of CL. The chirality of the experimentally obtained vortex-arrays with different singularity is stable once the laser oscillates. The chirality of the vortex-array is controlled by tilting the output coupler with respect to the Nd:YAG/Cr^{4+}:YAG composite crystal, which is similar to the chirality control in the annular beam pumped Cr,Nd:YAG self-Q-switched microchip laser [34]. Therefore, one-dimensional vortex-arrays with tunable singularity from one to four and stable chirality were achieved in DAB pumped tilted PQS microchip laser. The switch of vortex-arrays can be easily achieved by adjusting the pump power and offset distance of CL in DAB pumped tilted PQS microchip laser.

3.3. Performance of PQS microchip lasers

A. Tilted PQS microchip laser

The average output power of tilted PQS microchip laser pumped with an annular beam was measured at different P_{in}s. The threshold pump power was measured to be 1.35 W. The linear increase of average output power with P_{in} is observed, as shown in Fig. 4. The slope efficiency (η_S) is 18.5%. The maximum average output power was 0.85 W when P_{in} was 5.66 W. The optical-to-optical efficiency was 15%.

Fig. 5 shows the pulse characteristics as a function of P_{in} for annular beam pumped tilted PQS microchip laser. The pulse energy increases slowly with P_{in} and then tends to be a constant when P_{in} is higher than 3 W. The Cr^{4+} ions saturable absorber is bleached with high intracavity intensity achieved when P_{in} is higher than 3 W. Therefore, the pulse energy is kept constant because the energy stored in Nd:YAG crystal is fully extracted. The maximum pulse energy was 19.7 μJ at

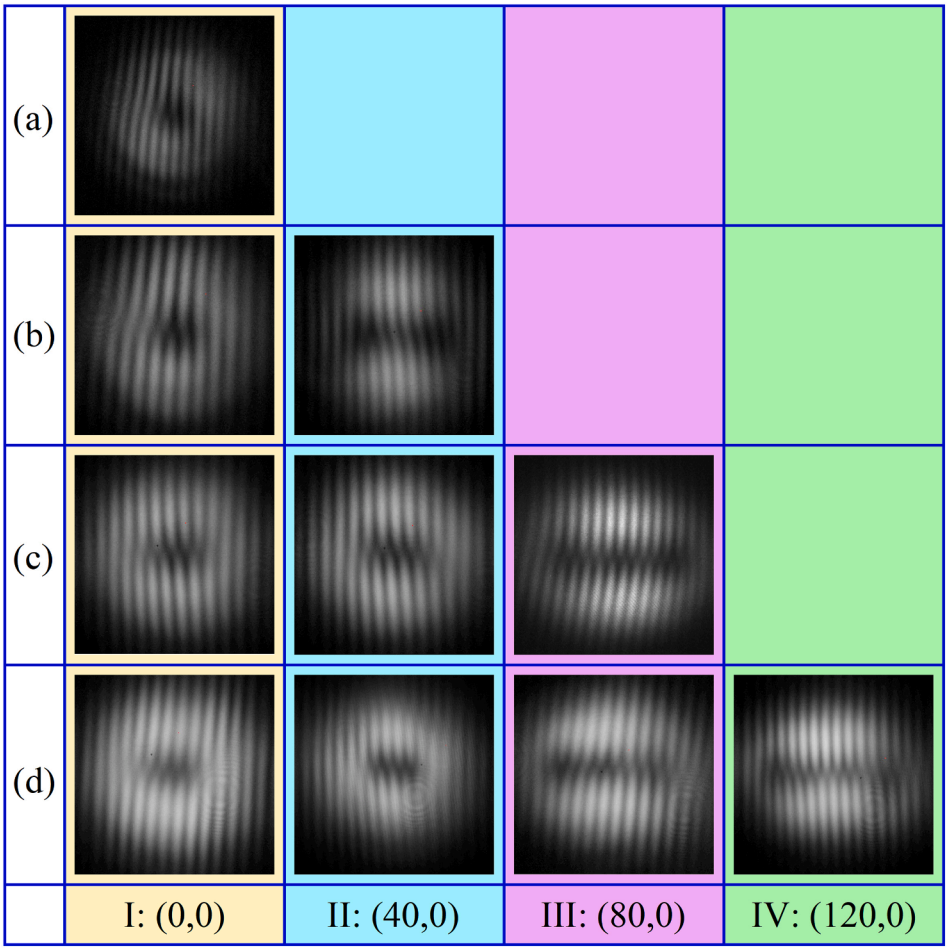

Fig. 3. Typical interference fringes of one-dimensional vortex-arrays with tunable singularity obtained experimentally in DAB pumped tilted PQS microchip laser at different P_{in}: (a) 1.37 W, (b) 2.48 W, (c) 3.81 W, (d) 5.21 W. (Δx,0) indicates the position of CL away from the propagation direction of fiber coupled LD, I: $\Delta x = 0$, II: $\Delta x = 40$ μm, III: $\Delta x = 80$ μm, IV: $\Delta x = 120$ μm.

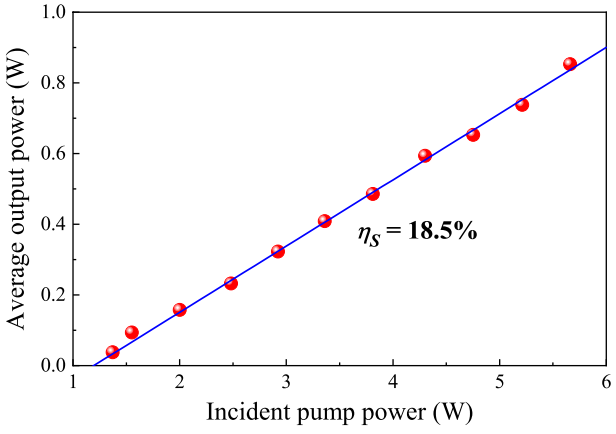

Fig. 4. Average output power as a function of P_{in} for tilted PQS microchip laser pumped with an annular beam and linearly fitted with a solid line.

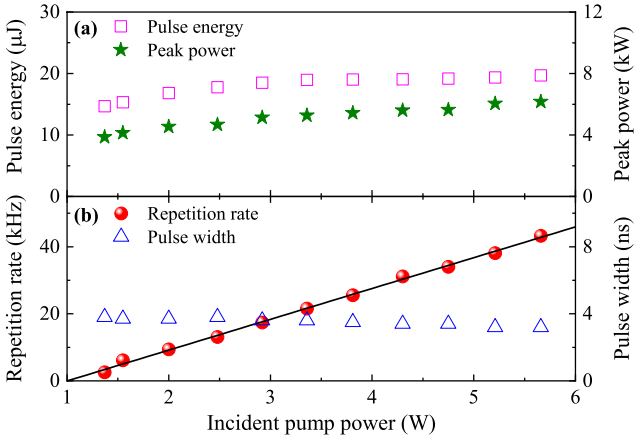

Fig. 5. (a) Pulse energy and peak power, (b) Repetition rate and pulse width as a function of P_{in} for annular beam pumped tilted PQS microchip laser.

P_{in} = 5.66 W. The peak power has almost the same variation trend as the pulse energy. The highest peak power was 6.16 kW at P_{in} = 5.66 W. The repetition rate increases linearly with P_{in} with a rate of 9.2 kHz/W. The highest repetition rate was 43.28 kHz when P_{in} was 5.66 W. The pulse width decreases slightly with P_{in} and then nearly keeps a constant around 3.2 ns when P_{in} is higher than 3 W.

B. DAB pumped tilted PQS microchip laser

The effect of offset distance of CL, Δx, on the performance of DAB pumped tilted PQS microchip laser was studied at two incident pump powers (P_{in} = 4.3 W and 5.66 W). The average output powers as a function of Δx at different P_{in}s are shown in Fig. 6. The average output power decreases slightly with Δx for different P_{in}s. For P_{in} = 4.3 W,

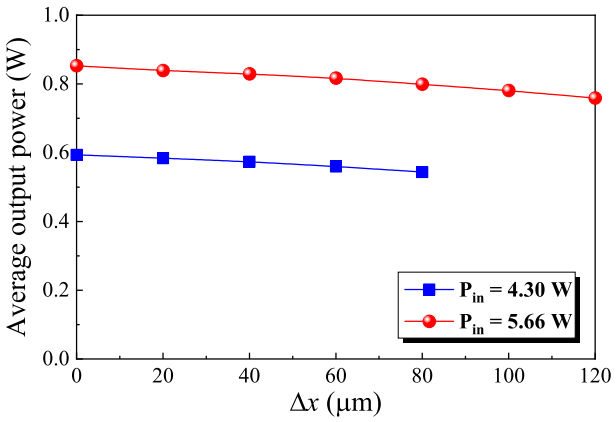

Fig. 6. Average output power of DAB pumped tilted PQS microchip laser as a function of Δx, P_{in} is fixed at 4.3 W and 5.66 W, respectively.

when Δx is tuned from 0 to 80 μm, the average output power drops only 6.7% from 0.594 W to 0.554 W. For P_{in} = 5.66 W, the average output power drops 11% from 0.85 W to 0.76 W when Δx is changed from 0 to 120 μm. Therefore, the performance of DAB pumped tilted PQS microchip laser is less affected by the offset distance of CL, Δx. Meanwhile, one-dimensional vortex-arrays with four singularity has been achieved by offsetting CL and increasing pump power.

Fig. 7 shows the pulse characteristics of DAB pumped tilted PQS microchip laser as a function of Δx for different P_{in}s. The repetition rate decreases by 7.8% from 31.18 kHz to 28.75 kHz for P_{in} = 4.3 W when Δx increases from 0 to 80 μm, while the repetition rate decreases 9.8% from 43.38 kHz to 39.02 kHz for P_{in} = 5.66 W when Δx increases up to 120 μm. The pulse width nearly keeps around 3.5 ns independent on Δx for P_{in} = 4.3 W, while the pulse width expands slightly from 3.2 to 3.5 ns when Δx is tuned up to 120 μm for P_{in} = 5.66 W. The slightly broadening of the pulse width at high pump power is caused by the enhanced thermal effect induced increase of the initial transmission of the Cr^{4+}:YAG saturable absorber. The pulse energy nearly keeps around 19 μJ and 19.7 μJ independent on the Δx for P_{in} = 4.3 W and P_{in} = 5.66 W, respectively. The peak power keeps a constant around 5.4 kW for P_{in} = 4.3 W when Δx increases from 0 to 80 μm, while the peak power decreases slightly from 6.16 kW to 5.56 kW for P_{in} = 5.66 W when Δx increases from 0 to 120 μm. The slight decrease in peak power is caused by the broadening of the pulse width induced by the increase of the initial transmission of Cr^{4+}:YAG saturable absorber.

From the experimental results of one-dimensional vortex-arrays with tunable singularity from 2 to 4 generated in DAB pumped tilted PQS microchip laser at P_{in} = 5.66 W by increasing Δx from 0 to 120 μm, we can see that one-dimensional vortex-arrays with singularity more than 4 is possible by further increasing pump power and Δx. Of course, the singularity of one-dimensional vortex-arrays can be further enlarged by adjusting the tilting angle of PQS microchip laser. Nanosecond, high peak power one-dimensional vortex-arrays with tunable singularity are laser sources for potential applications such as high capacity optical communication, quantum entanglement, assemble material processing, and optical tweezers.

4. Theoretical simulations

Formation of laser transverse patterns in an optical pumped solid-state laser resonator is mainly governed by the gain distribution and losses. The intensity distribution of annular pump beam formed with an HFL is similar to that of a $LG_{0,1}$ beam. The gain of a resonator is proportional to the inversion population excited by the pump power. Therefore, for DAB pumped tilted PQS microchip laser pumped at an incident pump power (P_{in}), the inversion population distribution in a gain medium is expressed as

$$\Delta N(x,y,z) = \frac{2P_{in}\alpha\tau\left[y^2 + (-z\sin(\theta+\beta) + x\cos(\theta+\beta))^2\right]}{h\nu_p\pi w_p^4\left[z\cos(\theta+\beta) + x\sin(\theta+\beta)\right]}$$

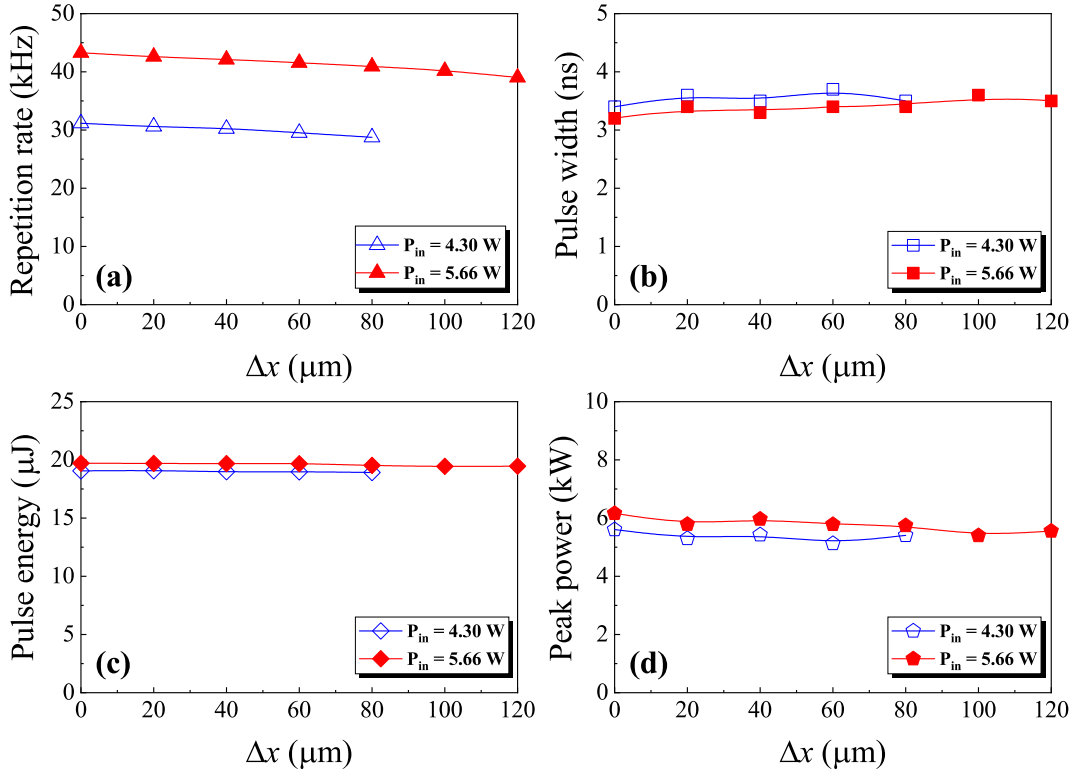

Fig. 7. (a) Repetition rate, (b) pulse width, (c) pulse energy and (d) peak power as a function of Δx. The P_{in}s are fixed at 4.3 W and 5.66 W, respectively.

$$\times exp\left[\frac{-2\left(y^2+\left(-zsin(\theta+\beta)+xcos(\theta+\beta)\right)^2\right)}{w_p^2[zcos(\theta+\beta)+xsin(\theta+\beta)]}\right]exp\left(\frac{-\alpha z}{cos(\theta+\beta)}\right) \quad (1)$$

where α and τ are absorption coefficient and fluorescence lifetime of gain medium, $h\upsilon_p$ is pump photon energy, $w_p[zcos(\theta + \beta) + xsin(\theta + \beta)]$ is the position dependent beam waist. The Δx-dependent tilted angle of decentered annular beam, θ, is expressed as

$$\theta(\Delta x) = \frac{z_1\Delta x}{f_1 f_2} - \frac{\Delta x}{f_1} \quad (2)$$

where z_1 is the distance between the collimating lens CL and hollow focus lens HFL, f_1 and f_2 are the focal length of CL and HFL, respectively.

The spatially distributed inversion population inside the gain medium determines the oscillation of different transverse modes, the effective inversion population averaged inside the gain medium is more accurate and convenient to reflect the position-dependent gain distribution for different transverse mode oscillation, and is expressed by averaging along the thickness of gain medium (l),

$$\Delta N_{eff}(x,y) = \int_0^l \Delta N(x,y,z)dz/l \quad (3)$$

The theoretically calculated saturated inversion populations along the thickness of Nd:YAG crystal at different P_{in}s are shown in Fig. 8. During the theoretical simulation, the Nd:YAG crystal is tilted 1° with respect to x-axis, the focus spot is set 0.3 mm away from the Nd:YAG crystal. When P_{in} is set to 2 W, the distribution of inversion population in the laser crystal is distorted along the crystal length, as shown in Fig. 8 (a1). The inversion population decreases gradually along the crystal length. Since the focus spot is located outside the Nd:YAG crystal, the pumped area expands along the thickness of Nd:YAG crystal. The effective inversion population distribution in x-y plane, as shown in Fig. 8(a2), is distorted and becomes an elongated ring along x-axis. When P_{in} is increased to 4 W, the distribution of inversion population along the crystal length is kept (Fig. 8(b1)). The distorted gain area with inversion population exceeding initial inversion population required for laser oscillation increases with P_{in}, which is favorable for multiple transverse modes oscillation. Therefore, dual-vortex laser is achieved in tilted PQS microchip laser. The gain distribution in the PQS microchip laser is greatly affected with the tilted laser resonator. The gain exhibits an elongated elliptic distribution in the tilted PQS microchip laser, therefore, the symmetry of the laser cavity is broken, and is favorable for dual-vortex laser oscillation. The enlarged spatial gain distribution region provides possibilities for high-order transverse mode oscillation. Further increase P_{in} to 6 W, the distribution of the inversion population, as shown in Fig. 8(c1), is similar to those at P_{in} = 2 W and 4 W. The oscillation of high-order transverse modes with enhanced effective inversion population, as shown in Fig. 8(b2) and (c2) makes dual-vortex laser oscillating in annular beam pumped tilted PQS microchip laser. From theoretical simulated results, we can see that P_{in} has a great influence on the spatial gain distribution. The spatial distribution of the gain inside the laser crystal expands gradually along the z-axis and x-y plane. Due to the high pumping intensity, the spatial gain distribution region with inversion population exceeding initial inversion population required for PQS laser oscillation expands and is favorable for high power dual-vortex laser operation.

The inversion population distribution along the Nd:YAG crystal thickness and the effective inversion population in the DAB pumped tilted PQS microchip laser is theoretically calculated at different offset distance of CL, Δx. The incident pump powers are set to 2.5 W and 5.5 W in the theoretical simulations. Fig. 9(a) shows the evolution of the

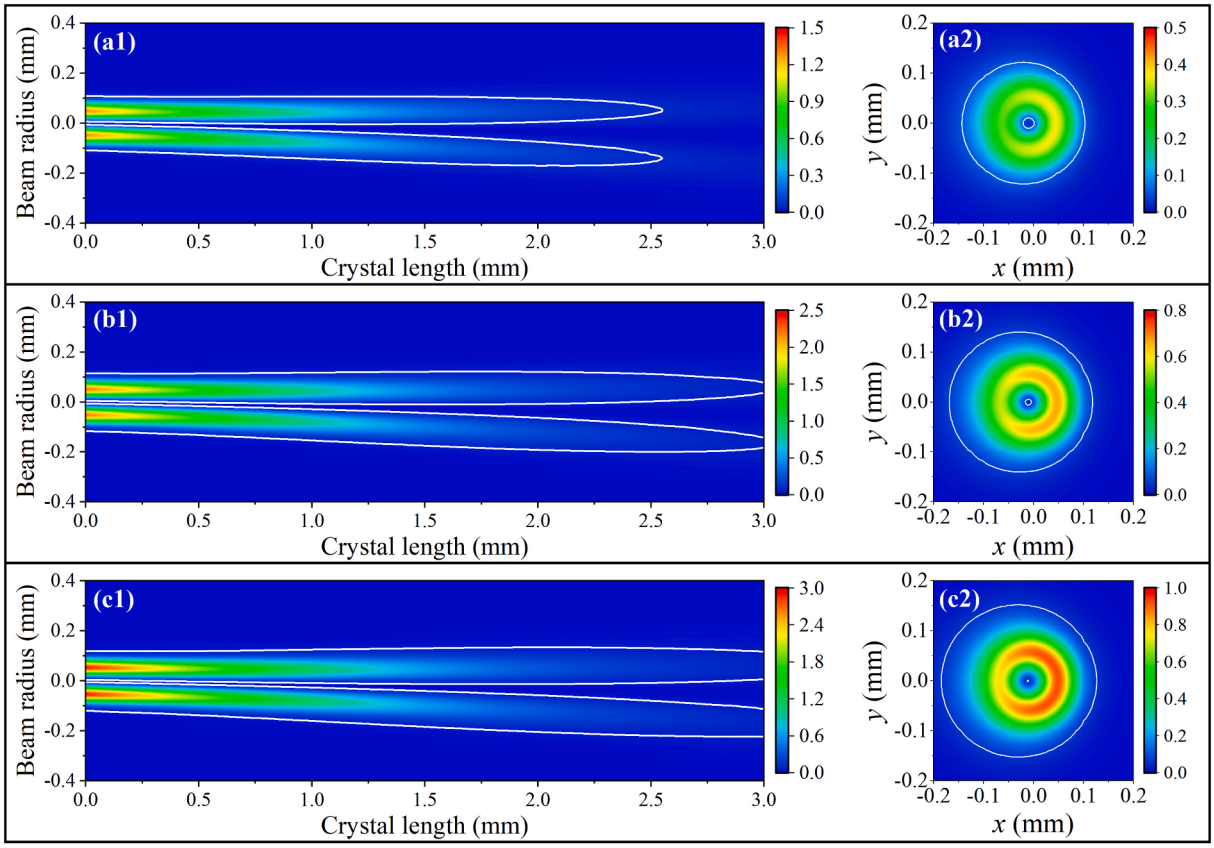

Fig. 8. Numerically simulated inversion population distribution inside Nd:YAG crystal tilted 1° with respect to x-axis. The P_{in} used in the simulations are: (a) 2 W, (b) 4 W, (c) 6 W. The solid lines are the initial inversion population for laser oscillation. The corresponding effective inversion population distribution is shown in the second column. The unit of the inversion population is $\times$ 10^{20} cm^{-3}.

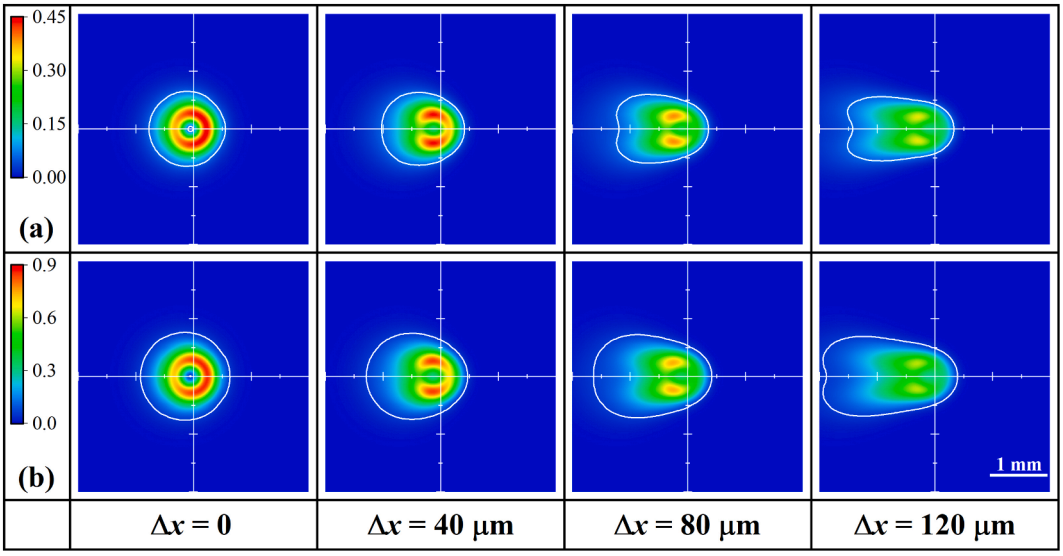

Fig. 9. Numerically simulation of the effective inversion population distribution for a 3-mm-thick Nd:YAG crystal at different offsets of CL along *x*-axis: $\Delta x = 0$, 40 μm, 80 μm, and 120 μm. The P_{in}s are set to (a) 2.5 W and (b) 5.5 W in the theoretical simulation. The initial inversion population for laser oscillation is shown in solid lines. The unit of the inversion population is $\times 10^{20}$ cm^{-3}.

effective gain distribution with Δx at $P_{in} = 2.5$ W. The effective gain distribution changes from a distorted ring with asymmetric distribution along *x*-axis at $\Delta x = 0$ to an elongated distorted elliptical ring when Δx is set at 40 μm. Further increasing Δx, the effective inversion population further expands along *x*-axis and becomes an elongated ring, as shown in Fig. 9(a) at $\Delta x = 80$ μm and 120 μm. However, the inversion population decreases with increasing of Δx because the gain area increases with Δx for the decentered annular beam. The effective inversion population is further enhanced by increasing P_{in}. As indicated in Fig. 9(b), the area of the effective inversion population distributions at different Δx expands and the profiles at different Δx are dramatically changed when the P_{in} is increased to 5.5 W. The effective inversion population increases about one-fold of those at $P_{in} = 2.5$ W for the same Δx. Therefore, elongated gain region with sufficient inversion population supports multiple transverse modes oscillation simultaneously for generating one-dimensional vortex-arrays in DAB pumped tilted PQS microchip laser. The elongated ring-shaped gain region is favorable for different LG modes oscillation. Therefore, the one-dimensional vortex-arrays with tunable singularity generated in DAB pumped tilted PQS microchip laser can be expressed with linear combination of LG modes.

The theoretically simulated intensity profiles of one-dimensional vortex-arrays with different singularities are depicted in Fig. 10(a1)-

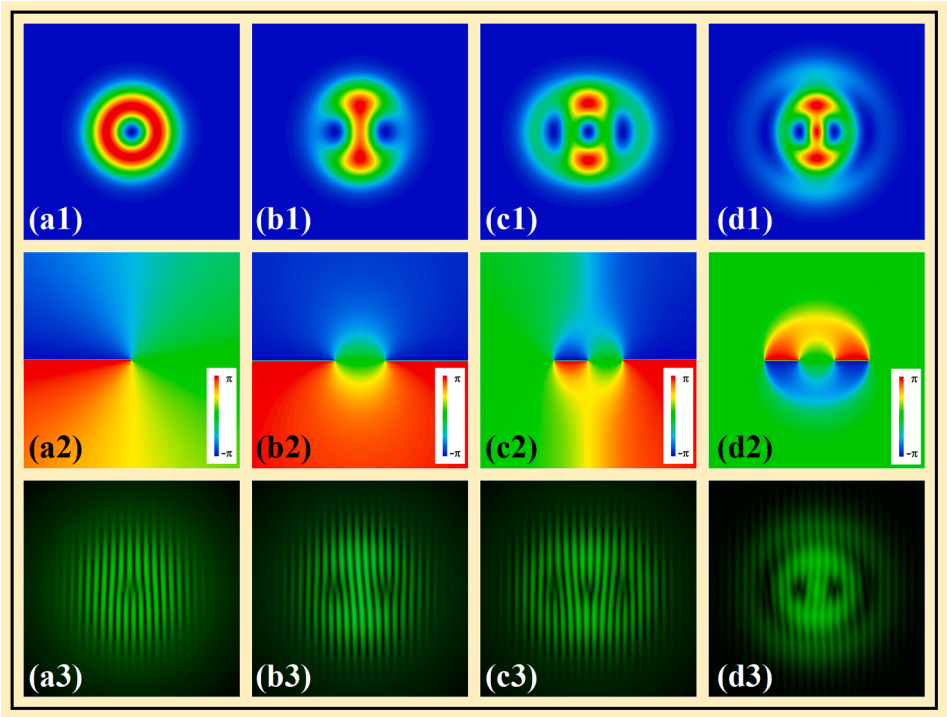

Fig. 10. Theoretically simulated intensity profiles (a1-d1), phases (a2-d2) and interference fringes (a3-d3) of one-dimensional vortex-arrays with singularity tuning from 1 to 4.

(d1). The intensity profile of vortex with one singularity is expressed as $|LG_{0,1}|$. The intensity profile of vortex-array with two singularities is expressed as $|g_1 \cdot LG_{1,0} + g_2 \cdot LG_{0,1} + g_3 \cdot LG_{0,-1}|$, where $g_1 = 1$, $g_2 = g_3 = 0.625$. The vortex-array with three singularities is expressed as $|g_1 \cdot LG_{1,1} + g_2 \cdot LG_{1,-1} + g_3 \cdot LG_{0,1} + g_4 \cdot LG_{0,-1}|$, where $g_1 = 1$, $g_2 = 0.4$, $g_3 = g_4 = 1$. The vortex-array with four singularities is expressed as $|g_1 \cdot LG_{2,0} + g_2 \cdot LG_{0,2} + g_3 \cdot LG_{0,-2} + g_4 \cdot LG_{0,1} + g_5 \cdot LG_{0,-1}|$, where $g_1 = 1$, $g_2 = g_3 = 0.6$, $g_4 = g_5 = 0.16$. The theoretically calculated intensity profiles are in good agreement with the experimentally obtained intensity profiles for the one-dimensional vortex-arrays with singularity of 1, 2 and 3. While the theoretical simulated intensity profile is in fair agreement with experimental result for one-dimensional vortex-array with four singularity. Thus, the formation of one-dimensional vortex-arrays with tunable singularity in DBA pumped tilted PQS microchip laser is simultaneous oscillation of LG modes spatially supported with elongated gain distribution in Nd:YAG crystal.

As shown in Fig. 10(a2), the phase changes from -π to π counterclockwise around singularity for doughnut vortex. From Fig. 10(b2), we can see that the phase varies 2π around two singularities for vortex-array, however, the variation of the phase is opposite for two singularities. From Fig. 10(c2), 2π variation of phase is observed around three singularities for vortex-array with three singularities, however, phase variation is opposite for two adjacent singularities. From Fig. 10(d2), we can see that phase varies 2π around four singularities for one-dimensional vortex-array with four singularities, and the phase variation between adjacent singularities is opposite. The calculated phases clearly confirmed that the one-dimensional vortex-arrays process phase singularities with unitary topological charge.

As shown in Fig. 10(a3)-(d3), forklike interference fringes with one fringe splitting into two fringes are formed at each singularity in the vortex-arrays. There is a topological charge for each singularity in the vortex-arrays. However, the orientations of the bifurcated forklike fringes are opposite for any two adjacent singularities in vortex-arrays with 2, 3 and 4 singularities. This is to say that the signs of the topological charges are opposite. Therefore, for the vortex-arrays with 2 and 4 singularities, the total charge is 0; while for the vortex-arrays with 3 singularities, the total charge is 1. Theoretically simulated intensity profiles, interference fringes are in good agreement with experimentally obtained results for the one-dimensional vortex-arrays (Fig. 2 and Fig. 3). The theoretically simulated results further confirmed that simultaneous oscillation of multiple transverse modes is the main mechanism for generating one-dimensional vortex-arrays with tunable singularity in the DBA pumped tilted PQS microchip laser.

5. Discussion

Here, the possibility of applying tilted PQS microchip resonator and DAB pump scheme to generate vortex-arrays with different singularity distribution is discussed. From the experimental and theoretical simulated one-dimensional vortex-arrays generated in a DAB pumped tilted PQS microchip laser, we can expect that combination of tilted PQS microchip laser cavity with Δx-dependent DAB induced elongated gain region along x-axis enables generation of one-dimensional vortex-array with large singularity. The elongated gain region can be extended by increasing Δx along x-axis and applying high pump power, which is favorable for generating one-dimensional vortex-array with singularity larger than 4 in the tilted PQS microchip laser. In addition, the elongated gain region can be also extended by adjusting the tilting angle of the PQS microchip laser cavity.

We demonstrated controllable separation and orientation of two vortices in a DAB pumped Nd:YAG/Cr^{4+}:YAG PQS microchip laser by adjusting the offsets of CL along x-axis and y-axis [37]. However, the singularity is only 2. By tilting PQS microchip laser, we obtained one-dimensional vortex-array with 4 singularities in DAB pumped tilted PQS microchip laser. The results show that combination of tilted PQS microchip laser cavity with DAB pumping scheme is a solid and simple method for generating one-dimensional vortex-arrays with more singularity. The distinct distribution of singularity in vortex-arrays is expected to be generated in DAB pumped tilted PQS microchip laser by subtle adjusting the offset of CL along x-axis and y-axis.

The elongated gain region for one-dimensional vortex-array generation in tilted microchip laser can be further extended by using single-emitter laser diode as pump source. The high-brightness single-emitter laser diode has a rectangular intensity profile, which is more favorable to extend along one direction by controlling the offset of CL. Therefore, one-dimensional vortex-array with large singularity is expected in a tilted PQS microchip laser pumped with a DAB formed with a single-emitter laser diode and an HFL.

The peak power of DAB pumped tilted Cr^{4+}:YAG PQS Nd:YAG microchip laser can be improved by adopting Cr^{4+}:YAG crystal with low initial transmission. The pulse width and pulse energy are determined by the initial transmission of the saturable absorber, the low the initial transmission of the saturable absorber, the shorter pulse width is achieved and the higher pulse energy is obtained in PQS microchip laser.

6. Conclusion

In conclusion, we demonstrated a method to generate high peak power, one-dimensional vortex-arrays with tunable singularity via offsetting collimating lens in a tilted Nd:YAG/Cr^{4+}:YAG PQS microchip laser pumped with a DAB formed with an HFL. The singularity of one-dimensional vortex-arrays can be tuned from 1 to 4 by adjusting offset of the collimating lens, Δx. The formation of one-dimensional vortex-arrays with tunable singularity in PQS microchip laser is attributed to Δx-dependent elongated gain region induced by the decentered annular beam. Its validity is also confirmed by the theoretical simulation of the simultaneous oscillation of multiple transverse modes. One-dimensional vortex-array with four singularities has been obtained at $\Delta x = 120$ μm. The output power of one-dimensional vortex-array with four singularities was 0.76 W at $P_{in} = 5.66$ W. The optical efficiency was 13.4%. The laser pulse width is 3.5 ns and peak power is 5.56 kW. Decentered annular beam pumping has been demonstrated to be a solid and robust method for generating vortex-arrays with different singularity distribution in PQS microchip lasers. High peak power, nanosecond one-dimensional vortex-arrays with tunable singularity provide a potential arena for optical communication, quantum entanglement, and optical tweezers.

Declaration of Competing Interest

The authors declare that they have no known competing financial interests or personal relationships that could have appeared to influence the work reported in this paper.

Acknowledgements

This work was supported by the National Natural Science Foundation of China under Grant 61475130, Grant 61275143 and Program for New Century Excellent Talents in University under Grant NCET-09-0669. X. Wang would like to thank Dr. Dimeng Chen and Dr. Mingming Zhang for their help on experiments and useful discussion.

References

[1] R. Fickler, R. Lapkiewicz, W.N. Plick, M. Krenn, C. Schaeff, S. Ramelow, A. Zeilinger, Quantum entanglement of high angular momenta, Science 338 (6107) (2012) 640–643.
[2] R. Fickler, R. Lapkiewicz, M. Huber, M.P.J. Lavery, M.J. Padgett, A. Zeilinger, Interface between path and orbital angular momentum entanglement for high-dimensional photonic quantum information, Nat. Commun. 5 (2014) 4502.
[3] D.G. Grier, A revolution in optical manipulation, Nature 424 (6950) (2003) 810–816.
[4] S. Franke-Arnold, L. Allen, M. Padgett, Advances in optical angular momentum, Laser Photon. Rev. 2 (4) (2008) 299–313.

[5] M. Padgett, R. Bowman, Tweezers with a twist, Nat. Photonics 5 (6) (2011) 343–348.
[6] M. Woerdemann, C. Alpmann, M. Esseling, C. Denz, Advanced optical trapping by complex beam shaping, Laser Photon. Rev. 7 (6) (2013) 839–854.
[7] C.F. Kuo, S.C. Chu, Numerical study of the properties of optical vortex array laser tweezers, Opt. Express 21 (22) (2013) 26418–26431.
[8] B. Thide, H. Then, J. Sjoholm, K. Palmer, J. Bergman, T.D. Carozzi, Y.N. Istomin, N. H. Ibragimov, R. Khamitova, Utilization of photon orbital angular momentum in the low-frequency radio domain, Phys. Rev. Lett. 99 (8) (2007), 087701.
[9] J.A. Anguita, J. Herreros, I.B. Djordjevic, Coherent multimode OAM superpositions for multidimensional modulation, IEEE Photonics J. 6 (2) (2014) 7900811.
[10] Y. Yan, G.D. Xie, M.P.J. Lavery, H. Huang, N. Ahmed, C.J. Bao, Y.X. Ren, Y.W. Cao, L. Li, Z. Zhao, A.F. Molisch, M. Tur, M.J. Padgett, A.E. Willner, High-capacity millimetre-wave communications with orbital angular momentum multiplexing, Nat. Commun. 5 (2014) 4876.
[11] A.E. Willner, H. Huang, Y. Yan, Y. Ren, N. Ahmed, G. Xie, C. Bao, L. Li, Y. Cao, Z. Zhao, J. Wang, M.P.J. Lavery, M. Tur, S. Ramachandran, A.F. Molisch, N. Ashrafi, S. Ashrafi, Optical communications using orbital angular momentum beams, Adv. Opt. Photonics 7 (1) (2015) 66–106.
[12] J. Wang, Advances in communications using optical vortices, Photonics Research 4 (5) (2016) B14–B28.
[13] M. Brambilla, F. Battipede, L.A. Lugiato, V. Penna, F. Prati, C. Tamm, C.O. Weiss, Transverse laser patterns. I. Phase singularity crystals, Phys. Rev. A 43 (9) (1991) 5090–5113.
[14] V.Y. Bazhenov, M.S. Soskin, M.V. Vasnetsov, Screw dislocations in light wavefronts, J. Mod. Opt. 39 (5) (1992) 985–990.
[15] Y. Toda, S. Honda, R. Morita, Dynamics of a paired optical vortex generated by second-harmonic generation, Opt. Express 18 (17) (2010) 17796–17804.
[16] J.B. Gotte, K. O'Holleran, D. Preece, F. Flossmann, S. Franke-Arnold, S.M. Barnett, M.J. Padgett, Light beams with fractional orbital angular momentum and their vortex structure, Opt. Express 16 (2) (2008) 993–1006.
[17] A.M. Nugrowati, W.G. Stam, J.P. Woerdman, Position measurement of non-integer OAM beams with structurally invariant propagation, Opt. Express 20 (25) (2012) 27429–27441.
[18] I. Martinez-Castellanos, J.C. Gutierrez-Vega, Vortex structure of elegant Laguerre-Gaussian beams of fractional order, J. Opt. Soc. Am. A-Opt. Image Sci. Vis. 30 (11) (2013) 2395–2400.
[19] J.C. Tung, H.C. Liang, T.H. Lu, K.F. Huang, Y.F. Chen, Exploring vortex structures in orbital-angular-momentum beams generated from planar geometric modes with a mode converter, Opt. Express 24 (20) (2016) 22796–22805.
[20] A.P. Porfirev, S.N. Khonina, Simple method for efficient reconfigurable optical vortex beam splitting, Opt. Express 25 (16) (2017) 18722–18735.
[21] Y.J. Shen, Y. Meng, X. Fu, M.L. Gong, Hybrid topological evolution of multi-singularity vortex beams: generalized nature for helical-Ince-Gaussian and Hermite-Laguerre-Gaussian modes, J. Opt. Soc. Am. A-Opt. Image Sci. Vis. 36 (4) (2019) 578–587.
[22] E.G. Abramochkin, V.G. Volostnikov, Generalized Gaussian beams, J. Opt. A-Pure Appl. Opt. 6 (5) (2004) S157–S161.
[23] V.V. Kotlyar, S.N. Khonina, A.A. Almazov, V.A. Soifer, K. Jefimovs, J. Turunen, Elliptic Laguerre-Gaussian beams, J. Opt. Soc. Am. A-Opt. Image Sci. Vis. 23 (1) (2006) 43–56.
[24] V.V. Kotlyar, A.A. Kovalev, A.P. Porfirev, Vortex Hermite-Gaussian laser beams, Opt. Lett. 40 (5) (2015) 701–704.
[25] M.A. Bandres, J.C. Gutierrez-Vega, Ince-Gaussian beams, Opt. Lett. 29 (2) (2004) 144–146.
[26] M.D. Wei, Y.S. Lai, K.C. Chang, Generation of a radially polarized laser beam in a single microchip Nd:YVO_4 laser, Opt. Lett. 38 (14) (2013) 2443–2445.
[27] Z.Q. Fang, K.G. Xia, Y. Yao, J.L. Li, Radially polarized and passively Q-switched Nd:YAG Laser under annular-shaped pumping, IEEE J. Sel. Top. Quantum Electron. 21 (1) (2015) 1600406.
[28] T. Dietrich, M. Rumpel, T. Graf, M.A. Ahmed, Investigations on ring-shaped pumping distributions for the generation of beams with radial polarization in an Yb:YAG thin-disk laser, Opt. Express 23 (20) (2015) 26651–26659.
[29] D.J. Kim, J.W. Kim, W.A. Clarkson, Q-switched Nd:YAG optical vortex lasers, Opt. Express 21 (24) (2013) 29449–29454.
[30] H.S. He, Z. Chen, J. Dong, Direct generation of vector vortex beams with switchable radial and azimuthal polarizations in a monolithic Nd:YAG microchip laser, Appl. Phys. Express 10 (5) (2017), 052701.
[31] D.M. Chen, X.C. Wang, H.S. He, J. Dong, Vector vortices with tunable polarization states directly generated in a microchip laser, Appl. Phys. Express 12 (5) (2019), 052012.
[32] D. Chen, S. Cai, J. Dong, Highly efficient Yb:YAG microchip laser for direct generation of radially polarized vector vortices, Eng. Res. Express 2 (4) (2020), 045035.
[33] D. Chen, Y. Miao, H. Wang, J. Dong, Vortex arrays directly generated from an efficient diode-pumped microchip laser, J. Phys. Photonics 2 (3) (2020), 035002.
[34] H.S. He, Z. Chen, H.B. Li, J. Dong, Low-threshold, nanosecond, high-repetition-rate vortex pulses with controllable helicity generated in Cr, Nd:YAG self-Q-switched microchip laser, Laser Phys. 28 (5) (2018), 055802.
[35] M.M. Zhang, H.S. He, J. Dong, Decentered Gaussian beam pumped highly efficient passively Q-Switched microchip laser for controllable high-order transverse modes, IEEE Photonics J. 9 (2) (2017) 1501214.
[36] J. Dong, S.C. Bai, S.H. Liu, K.I. Ueda, A.A. Kaminskii, A high repetition rate passively Q-switched microchip laser for controllable transverse laser modes, J. Opt. 18 (5) (2016), 055205.
[37] Y. Pan, M.M. Zhang, J. Dong, Orientation and separation controllable dual-vortex passively Q-switched microchip laser, J. Opt. 21 (8) (2019), 085202.